Steel and Composite Structures, *Vol. 36, No. 2 (2020) 229-247*
DOI: https://doi.org/10.12989/scs.2020.36.2.229

Time-dependent analysis of slender, tapered reinforced concrete columns

Alexandre de Macêdo Wahrhaftig*

Federal University of Bahia (UFBA), Polytechnic School, Dept. of Construction and Structures, Rua Aristides Novís, 02, 5º andar, Federação, Salvador, BA, 40210-910, Brazil

(*Received January 22, 2020, Revised May 26, 2020, Accepted June 30, 2020*)

Abstract. This study analyzed stresses in concrete and its reinforcement, computing the additional loading transferred by concrete creep. The loading varied from zero, structure exclusively under its self-weight, up to the critical buckling load. The studied structure was a real, tapered, reinforced concrete pole. As concrete is a composite material, homogenizing techniques were used in the calculations. Due to the static indetermination for determining the normal forces acting on concrete and reinforcement, equations that considered the balance of forces and compatibility of displacement on cross-sections were employed. In the mathematical solution used to define the critical buckling load, all the elements of the structural dynamics present in the system were considered, including the column self-weight. The structural imperfections were linearized using the geometric stiffness, the proprieties of the concrete were considered according to the guidelines of the American Concrete Institute (ACI 209R), and the ground was modeled as a set of distributed springs along the foundation length. Critical buckling loads were computed at different time intervals after the structure was loaded. Finite element method results were also obtained for comparison. For an interval of 5000 days, the modulus of elasticity and critical buckling load reduced by 36% and 27%, respectively, compared to an interval of zero days. During this time interval, stress on the reinforcement steel reached within 5% of the steel yield strength. The computed strains in that interval stayed below the normative limit.

Keywords: critical buckling load; analytical solution; creep; geometric nonlinearity; material nonlinearity

1. Introduction

A column is a continuous structural compression member whose vibrations are described by nonlinear partial differential equations (Kumar and Pratiher 2019) for which exact analytical solutions cannot be determined (Awrejcewicz *et al.* 2015). According to Uzny (2011), the resistance of a column can be quantified in several ways, which are not exclusively based on the cross-section capacity as they must also account for buckling in slender members. A slender column reaches the ultimate limit state (ULS) due to loss of stability before it reaches the resistance of the section. Thus, the critical buckling load is an important design parameter for slender columns and was first investigated by Euler (1744), complemented by Greenhill (1881), and confirmed by Timoshenko and Gere (1961). Euler buckling, defined as the phenomenon wherein an elastic member bends under the action of a compressive axial load, has also been studied by Lubbers *et al*. (2017). According to Johnston (1983), who proposed a mathematical process for the historical development of the critical buckling load, the Euler load is defined as the critical force whereby a slender elastic column can be held in a bent configuration under only axial loading. Essentially, the currently accepted solution for buckling, which is very widely used in engineering problems, is based on the static equilibrium of forces at the most-used section of the column under the assumption of a specific bending type. Even though Euler's formula has been used up to now, its application to actual members with cross-section geometries that change along the length is extremely difficult. This fact has been highlighted by Bert (1984), who confirmed that applying the Euler process to stepped columns (symmetric or non-symmetric) and tapered (smooth) columns for determining the buckling load is extremely difficult. In two studies, Bert (1984, 1987) solved a series of buckling problems using Euler's (1744) and Rayleigh's (1877) principles but without considering the self-weight of the elements. The difficulty of including the self-weight of a column lies in the fact that the mathematical development relies on solving elliptic integrals. Hence, the self-weight of a cantilever column reduces the critical buckling load by one-third of the column's self-weight, Timoshenko and Gere (1961), and should not be disregarded in cases of slender columns. An enhanced description of the stability of slender columns under its own weight can be found in Murawski (2017).

As can be seen, the mathematical procedure for determining the critical buckling load was initially defined in the field of statics in rational mechanics. However, the loss of stability due to buckling is essentially a dynamic phenomenon whose solution is based on the stiffness and mass of the system. In this case, the structural stiffness must be composed of two terms, one corresponding to the conventional stiffness and another to the geometric stiffness. For columns made of reinforced concrete (RC), a composite material formed of a combination of steel and concrete, the procedure for calculating the critical buckling

*Corresponding author, Associate Professor
E-mail: alixa@ufba.br

ISSN: 1229-9367 (Print), 1598-6233 (Online)

load should take into account the properties of each material, including the rheological behavior of concrete. For these cases, it is possible to introduce in the first portion of the stiffness, a variable modulus of elasticity over time that allows accompanying the deformation increase according to the adopted criterion. Thus, the total stiffness takes the form in which the mathematical model used to represent the creep is introduced in the first part, and the second part is geometric and a function of the normal force acting on the system. The geometric stiffness is the one that univocally imposes buckling because it depends exclusively on the applied axial load and system geometry.

Due to concrete creep, some of the stresses that were initially resisted by this material are gradually transferred to the longitudinal reinforcement in the cross-sections, attributable to the hypothesis of perfect bonding between the concrete and the reinforcement steel at the interface so that no slip can occur between the two materials. With that, the translation of the referred sections is made equally for both materials. For this reason, it is necessary to apply the equilibrium equations of forces and displacement compatibility to obtain the induced stresses in each material. Some studies showed the possibility of the steel bars yielding due to the portion of stress transferred by concrete creep to the reinforcement. To evaluate this phenomenon, an analytical mathematical procedure was employed to investigate a real, reinforced concrete column for which the critical buckling load was dynamically determined.

In the dynamics field, columns are continuous systems, and their analysis can be reduced to an analogous system containing a single-degree-of-freedom. The buckled configuration modes are restricted to a configuration established using a mathematical function describing the vibratory movement, and the properties of the system can be expressed as generalized coordinate functions. Rayleigh (1877) investigated the vibration of elastic systems and applied this technique by considering that the function is valid throughout the problem domain. As pointed out by Banerjee and Ananthapuvirajah (2019) the results obtained for this method depend directly on the shape function used to derive the dynamic matrix. The dynamic matrix derived in this way contains both the mass and stiffness properties of the element, unlike a discretization method such as the finite element method (FEM), for which the accuracy of results is tied to the number of elements used in the analysis. However, it is important to note that, in actual cases, where the properties of the structural elements vary along their length, the formulation for calculating the stiffness and mass using Rayleigh's method must be solved by observing the intervals existing in the geometry.

To analytically define the critical buckling load for the case modeled in this study, all stiffness components were considered in the calculation, including conventional stiffness, which depends on the material behavior, and geometric stiffness, which depends on the normal force acting on the structure and must include the self-weight of the element under analysis. The soil beneath the foundation was also considered, accounting for soil-structure interaction. Therefore, this procedure entails geometric and material nonlinear analysis, with solutions obtained directly in the continuum without applying any interactive process.

However, the analysis of the buckling load in an RC circular section using an interactive process considering short- and long-term action has been carried out by Bradford and Gilbert (1992), who confirmed that, along with the second-order effect in the creep of a slender column, an additional loss of stiffness also occurs. Therefore, they homogenized the reinforcement at the cross-section and used the age-adjusted effective modulus method for the time effects, as has been proposed by Bazant (1972). Additionally, Bazant (1972) applied a variable modulus of elasticity to consider the unbounded creep phenomenon of concrete, which can be calculated using the superposition principle for the deformations over time, wherein there exists a linear relationship between the time deformation and creep coefficient. Subsequently, these principles were incorporated into the analysis of creep for RC structures post hoc (Kawano and Warner 1996, Maru *et al.* 2001, Sharma *et al*. 2004).

2. Motivation and relevance

Studies existing in the technical literature indicate the possibility of the steel bars yielding due to the portion of stress transferred by concrete creep to the reinforcement. Madureira *et al.* (2013) and Kataoka *et al.* (2014) investigated the occurrence of creep transfer to the reinforcement inside the compressive columns. The former study pointed out that slow deformation can be prolonged for 3000 days after the loading is applied. Madureira *et al.* (2013) investigated prismatic pieces with sections having a reinforcement ratio (ξ) between 0.40% and 1.58% using the Maxwell-Chain Model to represent concrete creep. They adopted in their analysis a convergence period after loading has been applied also of 3000 days. Although Kataoka *et al*. (2014) investigated short pillars with reinforcement ratios of 1.4% and 2.8%, they observed the existence of stress transfer to the reinforcement through experimental and numerical evaluations. However, the results obtained by modeling using the FEM did not agree with the experimental results.

In terms of time effect of the concrete strain, Fragiacomo *et al*. (2002) studied the influence of creep on steel-concrete composite beams, and Dezi *et al*. (2006) investigated premature cracking in a slab of tapered prefabricated bridge deck considering a linear viscoelastic function for concrete creep in early ages. By assuming a linear elastic theory for materials, Dezi *et al*. (2006) used an analytical formulation based on virtual displacements for predicting the evolution of a structure that undergoes complicated changes of geometry. In the previous studies, the hypothesis of a perfect bond between concrete and reinforcement was adopted. Creep overstresses the reinforcement until it eventually yields but relieves the concrete portion of the structure. Under sustained loading, there is a gradual transfer of load from the concrete to the reinforcement in the concrete columns, which may lead to the steel yielding in very slender columns, as confirmed by

Samral (1995), who also considered an RC section by homogenizing the steel-reinforced area. A similar procedure of homogenizing a section composed of different materials was used by Mirmiran (2001) when studying the bucking of concrete-filled fiber-reinforced polymer columns.

To evaluate aspects related to designing reinforced concrete structures, this study analyzes the limit state of longitudinal strains and stresses induced in the longitudinal reinforcement of cross-sections of a structure subjected to concrete creep. These aspects were mathematically evaluated using a model that consists of a very slender column, clamped at the base, and free at the upper end, which had a variable cross-section along the height. The study was carried out for an axial loading varying from zero, structure exclusively under its self-weight, to near the loss of stability by bifurcating equilibrium, using the critical buckling load defined by the concepts of vibration of structural systems.

A slender RC pole with variable geometry, for which the critical buckling load was calculated using a structural dynamic criterion was studied. The nonlinearity of the material was calculated by reducing its flexural stiffness, which reflects the development of cracks in the concrete, in combination with the mathematical model for creep, which complies with the guidelines of the American Concrete Institute (ACI 209R, 2008). Additionally, the geometric nonlinearity was mainly considered and solved by calculating the second-order geometric stiffness matrix. Therefore, the present analysis is a linearization of a nonlinear analysis. The importance of these nonlinear aspects in calculating the buckling load and analyzing the vibration of one-dimensional elements was highlighted by Wang *et al.* (2006), Afefy *et al.* (2016), and Awrejcewicz *et al.* (2019).

Although some studies existing in the technical review related to the subject reveal the possibility of reinforcement yield, at the end of the present study, it was possible to conclude that the stresses induced in the reinforcement, including the additional portions due to concrete creep, do not produce the yielding of the material.

3. Preliminary concepts

Creep represents an increase of deformation due to long-term loads (Jung *et al*. 2007). Even under constant stress, creep occurs in concrete structures due to their viscoelastic nature (Mehta *et al.* 1994). Slow deformation, or creep, is a time-dependent phenomenon related to loading and strain, and it is defined as the increase of deformation over time under the action of permanent loads or stresses. Creep produces permanent deformation, which can potentially alter the material characteristics and their mechanical properties and can even result in structural collapse. From a practical viewpoint, technical standards consider the phenomenon of creep in sizing structures from two aspects, either by proposing a coefficient of increasing or decreasing stiffness or by proposing a coefficient of increasing or decreasing resistance, according to the load duration and moisture condition. Finally, it is important to obtain a function describing the deformation of the element over time, which differs according to the calculation process. However, stress and strain analysis of a viscoelastic material can present many difficulties for real problems of complex geometry, Zienkiewicz *et al*. (1968).

In an analysis, structural elements, such as beams or columns, are characterized as continuous systems and can occasionally be subjected to the action of axial compressive forces. When these elements are slender, they can reach the ULS, defined as the loss of stability, without having exhausted the capacity of their cross-sections. This condition is called buckling and is defined as a phenomenon whereby a structural element loses its equilibrium or is bent under the action of a compressive axial force that is sufficiently large to displace the element from its initial straight configuration. This is the best-known criterion for verifying the safety of slender members, and its solution originated in the field of statics within the broader field of mechanics. However, buckling is essentially a dynamic problem because it involves the equilibrium (or vibration) of mechanical systems, which depends on stiffness and mass. Regardless of this being a static or dynamic problem, the stability verification of slender elements should consider all changes undergone by the material, including creep, throughout the lifetime of the material.

This inclusion, either by the static or dynamic path, can be made by observing the stiffness of the structure, which must comprise two terms, the conventional stiffness component (or matrix) and the geometric stiffness component (or matrix). Thus, it is possible to adapt the former term by introducing a modulus of elasticity that varies over time to accompany the increase of deformations according to the adopted criterion, whether normative or mathematical rheological models based on spring and dashpot, as suggested by Szyszkowski and Glockner (1985), who used rheological models for representing the concrete creep effect in column buckling analyses. Therefore, the total stiffness takes a form where the mathematical model used to represent the viscoelastic behavior of the material can be introduced into the first stiffness component through the modulus of elasticity. The latter term is a function of the normal force acting on the system.

Hence, in the ULS, it is important to consider the effect of creep on the stability of slender and compressed structural elements because the stiffness of these members is modified as a function of the material's rheology. For the correct analysis of these systems in any field, all aspects involving the stiffness of structural elements and the material variations, including the viscoelastic behavior, must be considered. Consequently, the problem of stability becomes a function of time and can be solved at any time instant.

The model chosen for considering the temporal variation of the modulus of elasticity of concrete in the present analysis is that specified by ACI 209R (2008), which recommends using a creep coefficient $\phi(t)$ in the increase of the initial elastic deformations. The creep coefficient is associated with a temporal modulus of elasticity of concrete, becoming a time-dependent problem, Eq. (1)

$$E(t)=\frac{E_{mct0}}{1+\phi(t)} \tag{1}$$

where E_{mct0} is the modulus of elasticity at the beginning of loading. To define the creep coefficient, ACI 209R (2008) provides the necessary parameters to the case specifically studied. Using a temporal modulus for the concrete has been used as a valid strategy for static and dynamic structural analysis. For example, Abderezak *et al*. (2017) employed this concept for studying stress on the interface of fiber-reinforced beams, considering creep in a time-dependent analysis.

4. Time-dependent dynamic solution near the loss of stability

4.1 Principle of virtual work

Fig. 1 shows the bar model of a structure in undamped free vibration, where t indicates the time dependency; this model represents the practical problem proposed in this analysis or any other similar unidimensional problem, where m_0 is a lumped mass at the tip, $u(t)$ and $q(t)$ denote the vertical and horizontal displacements of the free end, respectively, g is the acceleration of gravity, *Gr* indicates ground, *Spr* means spring, L is the length of the column, x represents the position of a generic section along the length, $v(x,t)$ is the local displacement to this reference, s is a segment defined between ordinates L_s and $L_{s\text{-}1}$, for which $N_s(x)$ is the force axially distributed, $k_{Sos}(x)$ is the spring stiffness, $\bar{m}_s(x)$ is the mass per unit length, $E_s(t)$ is the viscoelastic modulus of the material with respect to time, and $I_s(x,t)$ is the variable moment of inertia of the section along the segment and relative to the considered movement.

To approximate the motion of this system using an SDOF model, it is assumed that the system deflected in a single manner that is adequately chosen to represent the vibratory movement of the first mode of buckling. The shape function describing this deflection is defined as $\varphi(x)$, where x is an independent variable representing the location along the height of the column, and the amplitude of the motion is represented by the generalized coordinate $q(t)$. The shape function was then obtained by calculating the following dimensionless ratio

$$\varphi(x)=\frac{v(x,t)}{q(t)} \therefore v(x,t)=\varphi(x)q(t) \tag{2}$$

The equation of motion for this generalized system can be conveniently formulated using Hamilton's principle. Hence, the external virtual work done by the forces of inertia, W_E, can be expressed as

$$W_E=-\sum_{s=1}^{n}\int_{L_{s-1}}^{L_s}\bar{m}_s(x)\ddot{v}(x,t)\delta v(x,t)dx+ m_0\ddot{v}(x,t)\delta v(x,t). \tag{3}$$

The internal virtual work done by the flexural deformation, $W_I(t)$, is given by

$$W_I(t)=\sum_{s=1}^{n}\int_{L_{s-1}}^{L_s}E_s(t)I_s(x,t)v''\delta v''dx \tag{4}$$

and the work done by the deformation of the foundation springs, W_{Spr}, is given by

$$W_{Spr}=\sum_{s=1}^{n}\int_{L_{s-1}}^{L_s}k_{Sos}(x)v(x,t)\delta v(x,t)dx \tag{5}$$

To calculate the work done by the axially directed normal force, whose direction and amplitude remained unchanged during the response, it is necessary to evaluate the vertical component of the motion of the column tip. Following the procedure described by Timoshenko and Gere (1961), the total displacement $u(t)$ along the column is given by

$$u(t)=\frac{1}{2}\int_0^L v'(x,t)^2dx \therefore \quad \delta u=\int_0^L v'(x,t)\delta v'(x,t)dx. \tag{6}$$

Thus, the potential energy of the axial load can be derived from

$$W_N=\sum_{s=1}^{n}\int_{L_{s-1}}^{L_s}\left(N_0+\sum_{s+1}^{n}N_{s+1}+N_s(x)\right)v'(x,t)\delta v'(x,t)dx, \tag{7}$$

where

$$N_0=m_0g\ ,\quad N_s=\int_{L_{s-1}}^{L_s}\bar{m}_s(x)gdx\text{, and} \quad N_s(x)=\left[\bar{m}_s(x)\left(L_s-x\right)\right]g\ . \tag{8}$$

Therefore, the external and internal virtual work obeys the following relationships

$$W_E+W_N=W_I+W_{Spr} \tag{9}$$

which leads to

$$\begin{aligned}&-\sum_{s=1}^{n}\int_{L_{s-1}}^{L_s}\bar{m}_s(x)\ddot{v}(x,t)\delta v(x,t)dx+\\&m_0\ddot{v}(x,t)\delta v(x,t)+\\&\sum_{s=1}^{n}\int_{L_{s-1}}^{L_s}\left(N_0+\sum_{s+1}^{n}N_{s+1}+N_s(x)\right)v'(x,t)\delta v'(x,t)dx=\\&\sum_{s=1}^{n}\int_{L_{s-1}}^{L_s}E_s(t)I_s(x,t)v''\delta v''dx+\\&\sum_{s=1}^{n}\int_{L_{s-1}}^{L_s}k_{Sos}(x)v(x,t)\delta v(x,t)dx\end{aligned} \tag{10}$$

considering that

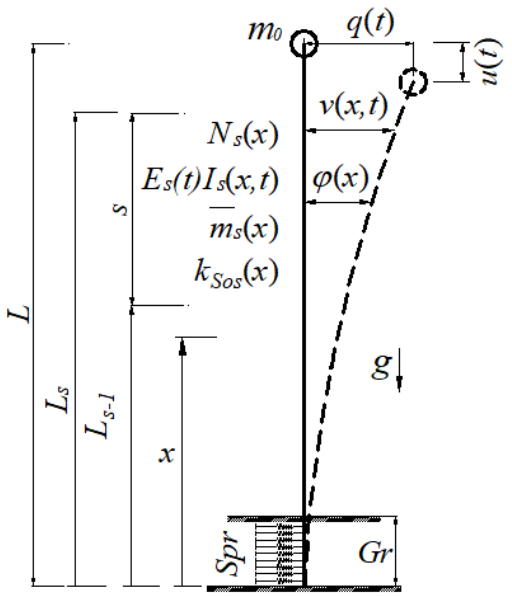

Fig. 1 Frame element model in free vibration

$$v'(x)=\frac{\partial v(x,t)}{\partial x},\quad v''(x)=\frac{\partial^2 v(x,t)}{\partial x^2},\quad \dot{v}(t)=\frac{\partial v(x,t)}{\partial t},\quad \ddot{v}(t)=\frac{\partial^2 v(x,t)}{\partial t^2}, \tag{11}$$

where $v'(x)$ and $v''(x)$ represent the first- and second-order derivatives, respectively, with respect to the independent variable of the lateral displacement, whereas $\dot{v}(t)$ and $\ddot{v}(t)$ represent the first- and second-order derivatives, respectively, with respect to the time elapsed during the lateral displacement. The real and virtual displacements and their derivatives, expressed as functions of generalized coordinates, as well as the shape functions used to represent the considered vibration modes, can be calculated using the following group of equations

$$\begin{aligned}
&v(x,t)=\varphi(x)q(t);\quad \dot{v}(x,t)=\varphi(x)\dot{q}(t);\quad \delta v'(x,t)=\varphi'(x)\delta q(t);\quad \dot{q}(t)=\frac{\partial q(t)}{\partial t};\\
&v'(x,t)=\varphi'(x)q(t);\quad \ddot{v}(x,t)=\varphi(x)\ddot{q}(t);\quad \delta v''(x,t)=\varphi''(x)\delta q(t);\quad \ddot{q}(t)=\frac{\partial^2 q(t)}{\partial t^2};\\
&v''(x,t)=\varphi''(x)q(t);\quad \delta v(x,t)=\varphi(x)\delta q(t);\quad \delta\dot{v}(x,t)=\varphi(x)\delta\dot{q}(t).
\end{aligned} \tag{12}$$

Substituting the appropriate terms from Eq. (12) into Eq. (10) yields

$$\left[\begin{aligned}
&\left(\sum_{s=1}^{n}\int_{L_{s-1}}^{L_s}\bar{m}_s(x)\varphi(x)^2dx+m_0\right)\ddot{q}(t)+\\
&\left(\sum_{s=1}^{n}\int_{L_{s-1}}^{L_s}E_s(t)I_s(x,t)\varphi''(x)^2dx\right)q(t)-\\
&\left(\sum_{s=1}^{n}\int_{L_{s-1}}^{L_s}\left(N_0+\sum_{j=s+1}^{n}N_j+N_s(x)\right)\varphi'(x)^2dx\right)q(t)\\
&+\left(\sum_{s=1}^{n}\int_{L_{s-1}}^{L_s}k_{Sos}(x)\varphi(x)^2dx\right)q(t)
\end{aligned}\right]\delta q(t)=0 \tag{13}$$

Because the variation, $\delta q(t)$, can assume any value, the term in brackets becomes zero and Eq. (12) can be rewritten as

$$M\ddot{q}(t)+K(t)q(t)=0 \tag{14}$$

where the generalized mass, M, of the system, including the mass at the tip, is given by

$$M=\sum_{s=1}^{n}\int_{L_{s-1}}^{L_s}\bar{m}_s(x)\varphi(x)^2dx+m_0 \tag{15}$$

and total stiffness, $K(t)$, is composed of three terms as follows

$$K(t)=K_0(t)-K_g+K_{So} \tag{16}$$

where the first term is the generalized conventional stiffness, $K_0(t)$, given by

$$K_0(t)=\sum_{s=1}^{n}\int_{L_{s-1}}^{L_s}E_s(t)I_s(x,t)\varphi''(x)^2dx \tag{17}$$

the second term is the geometric stiffness, K_g, given by

$$K_g=\sum_{s=1}^{n}\int_{L_{s-1}}^{L_s}\left(N_0+\sum_{s+1}^{n}N_{s+1}+N_s(x)\right)\varphi'(x)^2dx \tag{18}$$

and the third term is the elastic stiffness of the spring, K_{So}, given by

$$K_{So}=\sum_{s=1}^{n}\int_{L_{s-1}}^{L_s}k_{Sos}(x)\varphi(x)^2dx \tag{19}$$

4.2 Finite element method

According to Bathe and Wilson (1973), in terms of near the loss of stability, the relevant eigenvalues and eigenvectors can be obtained by solving the following secular equation

$$\left\{\left(K_0+K_{So}\right)-\left[\lambda\right]\left(K_g\right)\right\}\left[\psi\right]=0 \tag{20}$$

where the stiffness matrix includes the geometric stiffness term, K_g, formulated similarly to Eq. (33), having K_0, and K_{So} as the conventional and spring matrices, respectively. The last one is those that represent the soil-structure iteration, λ and ψ are the eigenvalues and eigenvectors related to the critical loads and their buckling shapes. The matrices present in Eq. (20) are defined for one single frame element of area A and length l, as indicated in Eqs. (21)-(23). The spring matrix is a six by six symmetric matrix of coefficients, k_{ij}, related to all translational and rotational degrees of freedom of a frame element. These matrices consider only one frame element and should be extrapolated to the global stiffness matrix, as proposed by the method. If a temporal problem is considered, a time variation of the parameter in the matrices should be introduced. A detailed development of the process for obtaining these matrices was presented by Wahrhaftig and Brasil (2017).

$$[K_{So}]=\begin{bmatrix} k_{11} & k_{12} & k_{13} & k_{14} & k_{15} & k_{16} \\ & k_{22} & k_{23} & k_{24} & k_{25} & k_{26} \\ & & k_{33} & k_{34} & k_{35} & k_{36} \\ & & & k_{44} & k_{45} & k_{46} \\ & \textit{symmetric} & & & k_{55} & k_{56} \\ & & & & & k_{66} \end{bmatrix} \tag{21}$$

$$[K_0]=E\begin{bmatrix} \frac{A}{l} & 0 & 0 & -\frac{A}{l} & 0 & 0 \\ & \frac{12I}{l^3} & \frac{6I}{l^2} & 0 & -\frac{12I}{l^3} & \frac{6I}{l^2} \\ & & \frac{4I}{l} & 0 & -\frac{6I(t)}{l^2} & \frac{2I}{l} \\ & & & \frac{A}{l} & 0 & 0 \\ & \textit{symmetric} & & & \frac{12I}{l^3} & -\frac{6I}{l^2} \\ & & & & & \frac{4I}{l} \end{bmatrix} \tag{22}$$

$$[K_g]=\frac{P}{l}\begin{bmatrix} 0 & 0 & 0 & 0 & 0 & 0 \\ & \frac{6}{5} & \frac{l}{10} & 0 & -\frac{6}{5} & \frac{l}{10} \\ & & \frac{2l^2}{15} & 0 & -\frac{l}{10} & -\frac{l^2}{30} \\ & & & 0 & 0 & 0 \\ & \textit{symmetric} & & & \frac{6}{5} & -\frac{l}{10} \\ & & & & & \frac{2l^2}{15} \end{bmatrix} \tag{23}$$

5. Application case

5.1 Generalized procedure

Let us consider the following trigonometric function, which is valid throughout the structure's domain

$$\varphi(x)=1-\cos\left(\frac{\pi x}{2L}\right) \tag{24}$$

where x is the location of the calculation and its origin is at the base of the cantilever, L is the length of the column, and $\varphi(x)$ is a function describing the vibratory movement. The trigonometric function in Eq. (24) was considered to be a function of x only, thereby effectively reducing the cantilever column to an SDOF system. The technique of using a shape function for describing a vibratory movement was introduced by Rayleigh (1877). As seen, the basic concept behind the Rayleigh method is the principle of conservation of energy in mechanical systems; therefore, it applies to linear and nonlinear structures. The purpose is to determine the fundamental period of vibration and to analyze the stability of the elastic systems with the precision required for engineering problems, Clough and Penzien (1993). According to Temple and Bickley (1933), this technique can be applied both to systems with finite degrees of freedom and continuous systems. Leissa (2005) notes that the precision obtained depends entirely on that function. If the exact shape is assumed, the exact corresponding frequency, or critical buckling load, is found by this method.

The method can be applied to any structure that can be converted in a unidimensional element, and sufficiently long to be bent. This model represents a column under an axial compressive load, with either constant or variable properties along its length, as seen in Fig. 1. These properties include geometry, elasticity/viscoelasticity, and density. Applied springs with variable stiffness act as lateral soil resistance at the foundation elevation. The system is under the action of gravitational normal forces, which originate from the mass distributed along the length of the column and the lumped mass at the tip. For the vibration of a cantilevered column that is clamped at its base but free at its tip, the shape function expressed by Eq. (24) satisfies the boundary conditions of the problem, i.e., when $x = L$ (at the free extremity of the column), $\varphi(L) = 1$, and when $x = 0$ (at the base), $\varphi(0) = 0$. Using Eq. (24) as a shape function for an actual structure with varying geometry for vibratory movements in the vicinity of the undistorted configuration was evaluated by Wahrhaftig (2019).

This evaluation involved a comparison to a computational solution obtained using computational modeling and other mathematical methods.

The dynamic properties of the subject system can be obtained by applying the principle of virtual work and its derivations, as previously described, similar to that done by Li *et al.* (2014). The elastic/viscoelastic conventional stiffness is expressed as follows

$$k_{0s}(t)=\int_{L_{s-1}}^{L_s} E_s(t)I_s(x,t)\varphi''(x)^2\,dx, \text{ with}$$
$$K_0(t)=\sum_{s=1}^{n} k_{0s}(t), \tag{25}$$

where, for a segment $s=L_s-L_{s-1}$ of the structure, $E_s(t)$ is the viscoelastic modulus of the material with respect to time, $I_s(x,t)$ is the variable moment of inertia of the section along the segment and relative to the considered movement, as obtained by interpolating the previous and following sections that are already homogenized with time (if it is geometrically constant along the length, it is simply denoted as $I_s(t)$), $k_{0s}(t)$ is the temporal term for the stiffness; $K_0(t)$ is the final conventional stiffness varying over time, and n is the total number of segment intervals determined by the structural geometry. In Eq. (25), t vanishes when the analysis considers a material with purely elastic, time-independent behavior.

The geometric stiffness appears as a function of the axial load, including the self-weight contribution, and is expressed as a function of the lumped mass at the tip, m_0, as follows

$$k_{gs}(m_o)=\int_{L_{s-1}}^{L_s}\left[N_0(m_o)+\sum_{s+1}^{n}N_{s+1}+\bar{m}_s(x)\left(L_s-x\right)g\right]\varphi'(x)^2\,dx \tag{26}$$

and

$$K_g(m_0) = \sum_{s=1}^{n} k_{gs}(m_0) \tag{27}$$

where $k_{gs}(m_0)$ is the geometric stiffness in segment s, $K_g(m_0)$ is the total geometric stiffness of the structure with n being as defined previously, $N_0(m_0)$ is the force concentrated at the top and is entirely dependent on the mass m_0 at the tip expressed, according to Eq. (28)

$$N_0(m_0) = m_0 g \tag{28}$$

and N_s is the normal force from the upper segments, as was already defined in Eq. (8) as follows

$$N_s = \int_{L_{s-1}}^{L_s} \bar{m}_s(x) g dx \tag{29}$$

Then, the total generalized mass, seen in Eq. (15), can be expressed as a dependent parameter of the lumped mass at the top, m_0, as follows

$$M(m_0) = m_0 + m \tag{30}$$

considering that the following relationship holds

$$m = \sum_{s=1}^{n} m_s \text{ , with } m_s = \int_{L_{s-1}}^{L_s} \bar{m}_s(x)\varphi(x)^2 dx \text{ , and}$$
$$\bar{m}_s(x) = A_s(x)\rho_s \tag{31}$$

where $\bar{m}_s(x)$ is the distributed mass to each segment s and is obtained by multiplying the cross-sectional area, $A_s(x)$, by the density, ρ_s, of the material in the respective interval. Therefore, $\bar{m}_s(x)$ is the mass per unit length and m is the generalized mass of the system, owing to the density of the material, with n being as previously defined. If the cross-section has a constant area over the interval, $A_s(x)$ will just be A_s; therefore, the distributed mass will also be constant. Similarly, if the mass, m_0, does not vary, all other parameters depending on it will also be constant.

One approach for considering the participation of the soil to the vibration of the system is to consider the soil as a series of vertically distributed springs acting as a restorative force on the system. Here, $k_{Sos}(x)$ denotes the spring parameter; the effective soil stiffness as a function of the location, x, along the length is defined as follows

$$k_{Sos}(x) = D_s(x) S_{ops}, \text{ what conducts to}$$
$$k_s = \int_{L_{s-1}}^{L_s} k_{Sos}(x)\varphi(x)^2 dx \text{ , and } K_{So} = \sum_{s=1}^{n} k_s \tag{32}$$

where parameter K_{So} is an elastic characteristic comprising the sum of k_s along the foundation depth, which depends on the geometry of the foundation, $D_s(x)$, and the soil parameter, S_{ops}. Moreover, parameter S_{ops} must be provided by a geotechnical engineer, and different methods are used by different geotechnical engineering specialists to determine this parameter.

Considering that the normal force is positive, the total structural stiffness can be obtained as follows

$$K(m_0, t) = K_0(t) - K_g(m_0) + K_{So} \tag{33}$$

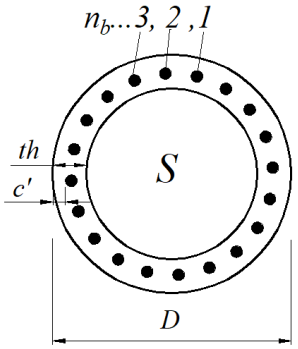

(a) Distribution of bars (*th* exist only for hollow sections)

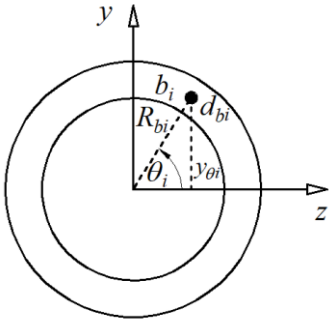

(b) Generic position of an i^{th} bar

Fig. 2 Typical cross-section adopted for the RC column

Finally, the natural frequency as a function of time and the mass at the tip is calculated in *Hz*, as follows

$$f(m_0, t) = \frac{1}{2\pi}\sqrt{\frac{K(m_0, t)}{M(m_0)}} \tag{34}$$

The mathematical procedure described above determines not only the frequency of a structure but also the critical buckling load because all generalized parameters are expressed as a function of the mass at the top. After introducing creep, the frequency and critical buckling load become temporal functions because the modulus of elasticity varies over time. Therefore, once creep is introduced into the calculation, the frequency can be written in terms of time and the mass at the top, as expressed by Eq. (34). Hence, the resultant expression is sufficient for calculating the critical buckling load, which is determined when the frequency is zero at any arbitrary time after the structure comes into service. The details of this analytical procedure can be found in Wahrhaftig *et al.* (2013, 2019). It should be noted that the results from the previous process are obtained directly in the continuum, without using any iterative process, as opposed to the analyses performed by Chaudhary *et al.* (2007) and Yaghoobi *et al.* (2014).

From the abovementioned considerations and by independently varying the lumped mass at the top of the structural pole, the force acting at the top and the frequency of the structure also vary. Thus, the critical buckling load, N_{cb}, is defined at zero frequency, as follows

$$N_{cb} = N_0(m_0)\big|_{f(m_0,t)=0} \tag{35}$$

The time dependence of the previous equations comes up due to the temporal nature of the homogenization factors between the elasticity moduli of steel and concrete, as seen in Eq. (1). To obtain these factors, consider the modulus of elasticity of the steel reinforcement, E^{st}. There are a number of bars, n_b, distributed along the periphery of the cross-section S (S varies from 1 to n, n represents the numbers of sections), of diameter D and wall thickness th if it is a hollow section, if not it is a full section and th is not applicable. c' is the concrete covering, and each bar has a diameter, d_{bi}, stated in Fig. 2(a). Each reinforcement bar, b_i, assumes a given position, i, in the cross-section domain, defined by R_{bi} and θ_i, as shown in Fig. 2(b). The variable R_{bi} describes the position of the barycenter of each bar, b_i, relative to the barycenter of the cross-section.
Because all the bars have the same radius, R_{bi}, Eq. (26) applies

$$R_{bi} = \frac{D}{2} - c' - \frac{d_{bi}}{2} \tag{36}$$

where c' is the covering of the section S and d_{bi} is the diameter of the ith bar.

Because θ_i is an independent variable that takes values between 0 and 2π, the distance between the center of each bar and the axis of the cross-section can be expressed as in Eq. (37)

$$y(\theta_i) = sin(\theta_i) R_{bi} \tag{37}$$

The spacing, sp, between the centers of adjacent bars is given by Eq. (38), where n_b denotes the number of longitudinal bars.

$$sp = \frac{2\pi R_{bi}}{n_b} \tag{38}$$

The angular phase shift, $\Delta\theta$, between two adjacent bars is given by Eq. (39)

$$\Delta\theta = \frac{sp}{R_{bi}} \tag{38}$$

The angular phase shift, $\Delta\theta$, between two adjacent bars is given by Eq. (39)

$$\Delta\theta = \frac{sp}{R_{bi}} \tag{39}$$

So, the moment of inertia of each bar about the cross-section barycenter, $I_i(\theta_i)$, can be calculated using Eq. (40)

$$I_i(\theta_i) = \frac{\pi {d_{bi}}^4}{64} + y(\theta_i)^2 \frac{\pi {d_{bi}}^2}{4} \tag{40}$$

The homogenized moment of inertia of the reinforcement steel over time, $I_h^{st}(t)$, can be expressed by Eq. (41)

$$I_h^{st}(t) = \sum_{\theta_i} I_i(\theta_i)\big(\eta(t) - 1\big) \tag{41}$$

where $\eta(t)$ is the temporal rate of the modulus of elasticity of the reinforcement steel and concrete, given by

$$\eta(t) = \frac{E^{st}}{E(t)} \tag{42}$$

where $E(t)$ is the time-dependent modulus of concrete as previously defined. To calculate the total homogenized moment of inertia $I_S^h(t)$ of the cross-section, it is necessary to consider Eq. (43)

$$I_S^h(t) = I_S + I_h^{st}(t) \tag{43}$$

where I_S is the non-homogenized geometric inertia of the cross-section, S, of concrete, calculated by Eq. (44) according to whether cross-section is hollow or full.

$$I = \frac{\pi}{64}\left[D^4 - \left(D - 2th\right)^4\right] or\ I = \frac{\pi}{64} D^4 \tag{44}$$

Therefore, the factors, $F_I^h(t)$, that multiply the moment of inertia of the section computed using the total moment of inertia of the reinforcement steel, can be written as in Eq. (45).

$$F_I^h(t) = 1 + \frac{I_h^{st}(t)}{I_S} \tag{45}$$

In the same direction, to homogenize the area of a cross-section, S, the total area of reinforcement should be considered using Eq. (46)

$$A_S^{st} = n_b \frac{\pi {d_b}^2}{4} \tag{46}$$

which takes the net area of concrete using Eq. (47)

$$A_{net}^c = A_S - A_S^{st} \tag{47}$$

where A_S is the area of the cross-section, S, calculated by Eq. (48) for each the type of section, hollow or full, as

$$A_S = \frac{\pi}{4}\left[D^2 - \left(D - 2th\right)^2\right] \text{ or } A_S = \frac{\pi}{4} D^2 \tag{48}$$

The homogenized area of reinforcement is given by

$$A_h^{st}(t) = A_S^{st}\left(\eta(t) - 1\right) \tag{49}$$

So, the temporal concrete homogenized area can be calculated using Eq. (50)

$$A_S^h(t) = A_S + A_h^{st}(t) \tag{50}$$

with $\eta(t)$ defined as in Eq. (42). The area homogenizing factors, $F_A^h(t)$, of section S are obtained through Eq. (51).

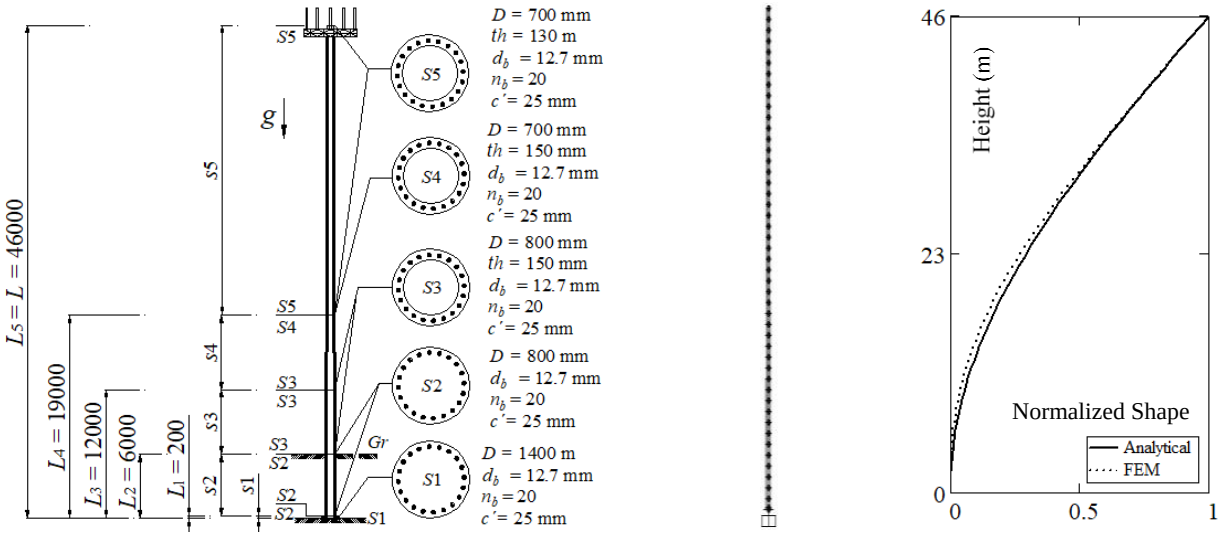

(a) Geometry and sections (heights in cm) (b) FEM (c) Shape functions

Fig. 3 Reinforced concrete pole

$$F_A^h(t) = 1 + \frac{A_h^{st}(t)}{A_S} \tag{51}$$

5.2 Specific procedure

The problem considered in this study entails calculating the critical buckling load for an actual extremely slender RC pole with variable geometry that exhibits geometrical and material nonlinearities. The structure is 46 m high, including a 40 m superstructure with a hollow circular section and a 6-m-deep, fully circular foundation. Here, the lateral soil resistance is represented by a unique elastic parameter, S_{op}, equal to 2669 kN/m^3 for all soil layers. The moduli of elasticity, E_{cmt0}, for the superstructure and foundation are 38240 MPa and 24040 MPa, respectively, and the characteristic compression resistance of concrete was assumed as 45 MPa and 20 MPa, respectively. The geometric details of the analyzed column are shown Fig. 3(a), where g and Gr were previously defined; s denotes each structural segment; S, D, and th are the type, external diameter, and wall thickness of the section, respectively; d_b represents the reinforcing bar diameter; n_b is the number of reinforcing bars; and c' is the reinforcing cover. The slenderness ratio of the concrete pole was 408, as calculated using a weighted average based on the geometry of the structure. A concentrated mass is commonly installed at the tip of the structure, whose value in relation to the loss of stability by buckling must be determined. An additional mass is also frequently installed along the entire length of the superstructure and joins a distributed mass, $\bar{m}_e$, of 40 kg/m to the system. The adopted densities for the superstructure and foundation were ρ = 2600 kg/m^3 and ρ_f = 2500 kg/m^3, respectively.

It is important to be clear that in the present analysis, concrete creep will be being directly considered in the modulus of elasticity for concrete. Additionally, the moment of inertia and area for every cross-section was increased to account for the reinforcing bars, according to Eq. (43). The viscoelastic aspect of the concrete was considered with regard to the superstructure, according to the ACI creep criteria. To consider concrete cracking, the factored moment of inertia was computed for all sections, with a 0.5 reduction factor for the gross moment of inertia (item ACI-6.6.3.1.2), although the possibility exists to use another reduction factor, as discussed by Marin and El Debs (2012). That factored moment of inertia was adopted considering that the structure will be under wind action, and for that reason, with forces acting laterally for bending it. This concept included the foundation, which was also considered in the vibratory movement, although confined in a certain way. If this factor is calculated according to ACI-Table 6.6.3.1.1(b), Eq. (52)

$$I_{fact} = 0.08 + 25\frac{A_S^{st}}{A_S} \tag{52}$$

where A_s is the gross concrete area of a section, S, and A_S^{st} is the reinforcement steel area, the factored averaged for cross-sections above terrain is 0.32 and 0.26 when are considering all cross-sections. However, it should be noted that the real cracking depends on the real forces acting on the structure.

A finite element analysis (FEA) was conducted to independently evaluate the results obtained by the analytical procedure previously presented. The considered structure was modeled using unidimensional elements with constant or variable cross-sections, as appropriate. The forces with corresponding masses were applied to the system. The spring factor was assigned to the foundation frame element as a linearly distributed parameter. Only a lateral spring was used to model the foundation system, and the spring stiffness matrix was, thus, considered to be null at all positions corresponding to the axial and rotational degrees of freedom, while the values extrapolated from the interior

of each element joint were considered to be active components of the matrix. Fig. 3(b) shows the discretization of the model constructed using SAP2000 (2019) structural analysis software, with the model discretized in 47 elements. Fig. 3(c) compares the shape function from FEA with that used in the analytical procedure, Eq. (24), which gives a relatively good agreement to the finite element solution, although there is a small difference at the middle of the height of the structure, can respond for some existent differences between methods. The processing was performed for each time, *t*, of interest. Therefore, the factors multiplying the nominal moment of inertia of the section in terms of the total moment of inertia in the homogenized sections were calculated according to parallel axis theorem, as specified previously, by Eq. (45). In the same way, the modulus of elasticity was calculated according to Eq. (1).

To apply the time-dependent solution development to the present case, the following order, referring to the heights in the structure, were defined as (sub-indices serve to identify a segment, *s*, as a section, *S*) $L_1 = 200\ mm$, $L_2 = 6000\ mm$, $L_3 = 12000\ mm$, $L_4 = 19000\ mm$, $L_5 = L = 46000\ mm$. On the base foundation, $D_1 = 140\ mm$, $A_1 = \frac{\pi}{4} D_1^{\,2}$, $I_1 = \frac{\pi}{64} D_1^{\,4}$. On the shaft $D_2 = 800\ mm$, $A_2 = \frac{\pi}{4} D_2^{\,2}$, $I_2 = \frac{\pi}{64} D_2^{\,4}$. The variable diameter between the base and the shaft is obtained by linear interpolation on the variable segment. So, the area and inertia of the section are given by $A_1(x) = \frac{A_2 - A_1}{L_1} x + A_1$ and $I_1(x) = \frac{I_2 - I_1}{L_1} x + I_1$. The external diameter and thickness of the third segment are $D_3 = 800\ mm$ and $th_3 = 130\ mm$. Then, the internal diameter, area, and inertia of the section are $d_3 = D_3 - 2th_3$, $A_3 = \frac{\pi}{4}\left(D_3^{\,2} - d_3^{\,2}\right)$, and $I_3 = \frac{\pi}{64}\left(D_3^{\,4} - d_3^{\,4}\right)$. The next section has an external diameter of $D_4 = 700\ mm$ and thickness equal to the previous one, $th_4 = th_3$. The fourth structural segment has a tapered section, its diameter can be obtained by linear interpolation, similarly as done for the first one. Therefore, $A_4(x) = \frac{A_4 - A_3}{L_4 - L_3}\left(x - L_3\right) + A_3$, and $I_4(x) = \frac{I_4 - I_3}{L_4 - L_3}\left(x - L_3\right) + I_3$ are, respectively, the area and the inertia of the variable section on the corresponding segment. Similarly, the external diameter, thickness, area, and inertia for the last segment are given by: $D_5 = 700\ mm$, $th_5 = 130\ mm$, $d_5 = D_5 - 2th_5$, $A_5 = \frac{\pi}{4}\left(D_5^{\,2} - d_5^{\,2}\right)$, and $I_5 = \frac{\pi}{64}\left(D_5^{\,4} - d_5^{\,4}\right)$. After defining the geometry, the generalized properties of the problem can be calculated.

The generalized mass is calculated by taking the following integrals and summing them to the end

$$
\begin{aligned}
&m_5 = \int_{L_4}^{L} \bar{m}_5 \varphi(x)^2\, dx \text{, with } \bar{m}_5 = A_5\rho + \bar{m}_e \text{;}\\
&m_4 = \int_{L_3}^{L_4} \bar{m}_4(x) \varphi(x)^2\, dx \text{, with } \bar{m}_4(x) = A_4(x)\rho + \bar{m}_e \text{;}\\
&m_3 = \int_{L_2}^{L_3} \bar{m}_3 \varphi(x)^2\, dx \text{, with } \bar{m}_3 = A_3\rho + \bar{m}_e \text{;}\\
&m_2 = \int_{L_1}^{L_2} \bar{m}_2 \varphi(x)^2\, dx \text{, with } \bar{m}_2 = A_2\rho_f \text{;}\\
&m_1 = \int_{0}^{L_1} \bar{m}_1(x) \varphi(x)^2\, dx \text{, with } \bar{m}_1(x) = A_1(x)\rho_f \text{; and}\\
&m = \sum_{s=1}^{5} m_s \text{.}
\end{aligned}
\tag{53}
$$

Adding the concentrated mass at the top, the total generalized mass, $M(m_0)$, is found using Eq. (30). The generalized geometric stiffness, $K_g(m_0)$, of the structure was obtained by summing these five terms

$$
\begin{aligned}
&K_{g5}(m_0) = \int_{L_4}^{L} \left[N(m_0) + \bar{m}_5 (L - x) g\right] \varphi'(x)^2\, dx \text{,}\\
&\text{with } N_0(m_0) = m_0 g \text{;}\\
&K_{g4}(m_0) = \int_{L_3}^{L_4} \left[N(m_0) + N_5 + \bar{m}_4(x)(L_4 - x) g\right] \varphi'(x)^2\, dx \text{,}\\
&\text{with } N_5 = \int_{L_4}^{L} \bar{m}_5 g dx \text{;}\\
&K_{g3}(m_0) = \int_{L_2}^{L_3} \left[N(m_0) + N_5 + N_4 + \bar{m}_3 (L_3 - x) g\right] \varphi'(x)^2\, dx \text{,}\\
&\text{with } N_4 = \int_{L_3}^{L_4} \bar{m}_4 g dx \text{;}\\
&K_{g2}(m_0) = \int_{L_1}^{L_2} \left[N(m_0) + N_5 + N_4 + N_3 + \bar{m}_2 (L_2 - x) g\right] \varphi'(x)^2\, dx \text{,}\\
&\text{with } N_3 = \int_{L_2}^{L_3} \bar{m}_3 g dx \text{;}\\
&K_{g1}(m_0) = \int_{0}^{L_1} \left[N(m_0) + N_5 + N_4 + N_3 + N_2 + \bar{m}_1(x)(L_1 - x) g\right] \varphi'(x)^2\, dx \text{;}\\
&\text{and } K_g(m_0) = \sum_{s=1}^{5} K_{gs}(m_0) \text{.}
\end{aligned}
\tag{54}
$$

By summing their components, the total generalized elastic stiffness, $K_0(t)$, is obtained by Eq. (55)

$$
\begin{aligned}
&K_{05}(t) = \int_{L_4}^{L} E(t) I_5(t) \varphi''(x)^2 dx \text{, with } I_5(t) = I_5^h(t) \text{;}\\
&K_{04}(t) = \int_{L_3}^{L_4} E(t) I_4(x,t) \varphi''(x)^2 dx \text{, with}\\
&I_4(x,t) = \frac{I_4^h(t) - I_3^h(t)}{L_4 - L_3}\left(x - L_3\right) + I_3^h(t) \text{;}
\end{aligned}
\tag{55}
$$

$$K_{03}(t)=\int_{L_2}^{L_3} E(t)I_3(t)\varphi''(x)^2dx \quad \text{with} \quad I_3(t)=I_3^h(t);$$

$$K_{02}=\int_{L_1}^{L_2} E_f I_2(t)\varphi''(x)^2\,dx, \text{ with } I_2(t)=I_2^h(t).$$

$$K_{01}=\int_{0}^{L_1} E_f I_1(x)\varphi''(x)^2\,dx, \text{ with}$$

$$I_1^h(x)=\frac{I_2^h-I_1^h}{L_1}x+I_1^h; \quad \text{and}$$

$$K_0(t)=\sum_{s=1}^{5}K_{0s}(t),$$

where E_f represents the modulus of the elasticity (E_{cmt0}) of the foundation, which is not a time-dependent parameter.

The total spring stiffness, K_{so}, of the soil can be expressed in terms of the distributed spring stiffnesses in the first and second segments, as follows

$$k_2=\int_{0}^{L_1} k_{So2}(x)\varphi(x)^2dx \quad \text{with} \quad k_{So2}(x)=D_2(x)S_{op};$$

$$k_1=\int_{0}^{L_1} k_{So1}(x)\varphi(x)^2dx, \text{ with } k_{So1}(x)=D_1(x)S_{op}; \text{ and} \quad (56)$$

$$K_{So}=\sum_{s=1}^{2}k_s$$

Once all terms of the generalized stiffness and mass are defined, the time-dependent vibration analysis can be performed according to Eqs. (34) and (35). Those equations represent the variation of the structural frequency in the time of interest as a dependent parameter of the force acting on the column top, for which its self-weight is already considered. By doing the concentrated mass in Eqs. (34) and (35) as the independent variable of the problem, this mass will be associated with the concentrated force acting on the free end, which can vary from zero up to the imminent loss of equilibrium. The loss of equilibrium is associated with the force that takes the structural frequency to null, as defined in Eq. (35). From there on, no more (even minimum) load can be applied, configuring a limit state. As the force on top varies, strain and stress on sections can be calculated until reaching their maximum possible values.

6. Results and discussion

The following conditions were assumed: cement type III, wet curing, slump standard (70 mm), 50% fine aggregate ratio, entrained air rate below 6%, and 70% environmental humidity. A study relating aggregate's influence on creep in a column was carried out by B-Jahromi *et al.* (2017). The variation of the effective modulus of elasticity over time is shown in Fig. 4(a). The continuous variation of the critical buckling load over time is described by the graph shown in Fig. 4(b). To obtain these results, a small programming routine was developed by considering a 0.1-kg increment for the mass at the top,

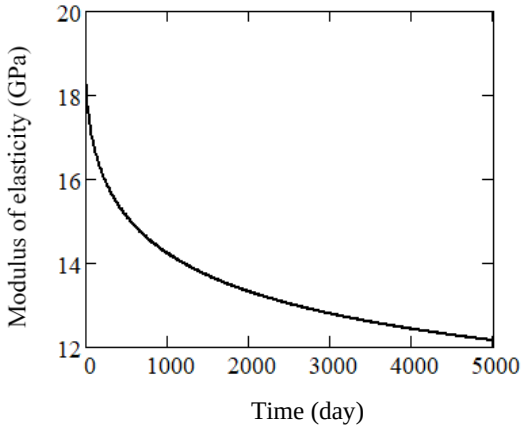

(a) Modulus of elasticity

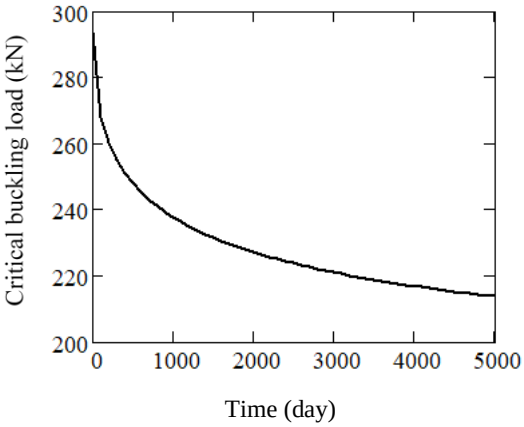

(b) Critical buckling load

Fig. 4 Modulus of elasticity of concrete and critical load over time

using a 10-day time-step, and adopting a 10^{-3} Hz precision for the frequency and an initial value for the mass at the tip of 19000 kg.

Under these conditions and using an Intel(R) Core (7M) 7500U CPU, 2.70–2.90 GHz, i7 (7th Generation) Intel processor operating on Windows 10 (64 bit) with 8 GB of memory (RAM), the total processing time was approximately 1 hour to the critical buckling load, and 5 hours to generate the graphic, for which a time-step of 100 days was used.

The variation of the structural frequency with the mass at the top of the structure is shown in Fig. 5(a), in which the critical buckling load can be obtained at any stage in the lifetime of the structure. In addition to the arbitrarily selected time intervals, the analysis could have been performed for any other moments of interest during the lifetime of the structure. However, 5000 days represents an appropriate design horizon, considering that in approximately one decade and a half, the technology changes and maintenance operations are needed. Even if a double length of time, 10000 days (~27 years), is considered as the lifetime of the structure, the critical buckling decreases by only 4.23%.

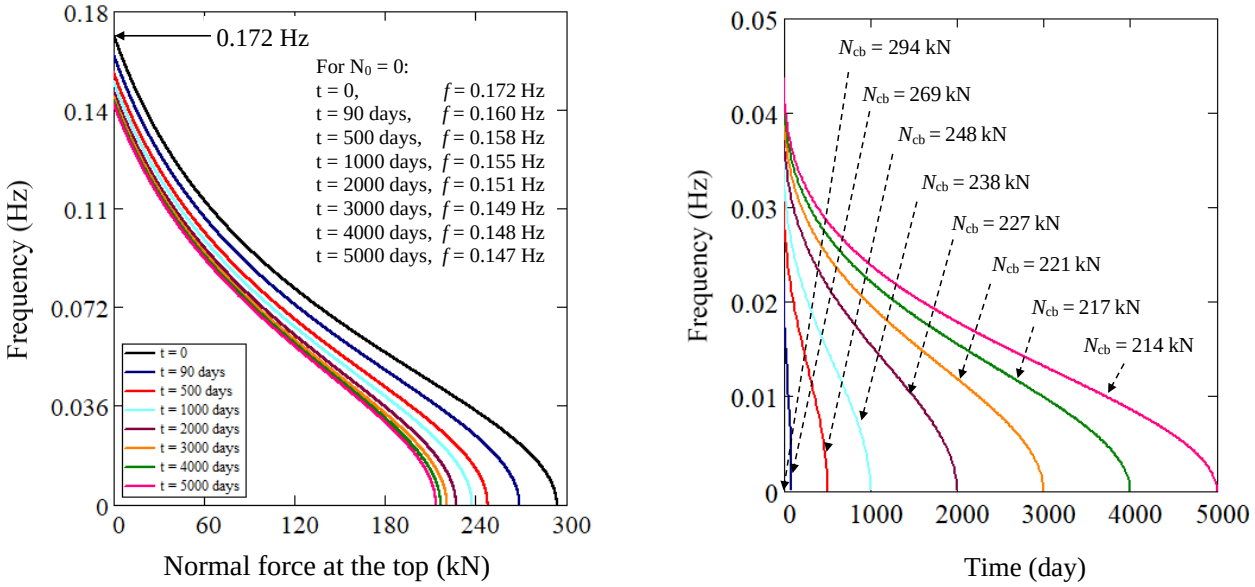

(a) Dynamically obtained critical buckling load (b) Frequency of critical buckling load over time

Fig. 5 Structural frequencies

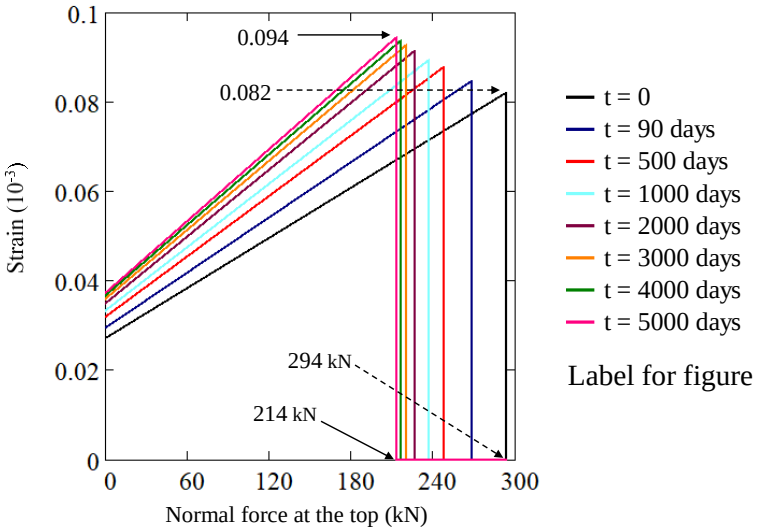

Fig. 6 Total structural strain over time according to the generalized normal force

If that time is 15000 days (~42 years), a reduction of 6.85% is found compared to 5000 days. Considering a later age, for instance, 20000 days (~55 years), the critical buckling load decreases just by 7.65%. In reality, the absolute convergence of results only occurs for an age that is out of the lifetime of the structure. The mass at the top can be obtained simply by dividing each buckling force by the acceleration of gravity.

Frequencies for the self-weight only can be seen in Fig. 5(a). From $t = 0$ (0.172 Hz) to 5000 days (0.147 Hz) there is a difference of around 2%. Fig. 5(b) shows the frequency variation of the structure over the considered time, as obtained by setting the normal force to the value corresponding to the critical buckling load. This graph is applicable for the case of temporary loading or use or even when the load to be applied is close to the maximum vertical loading structural capacity. The force corresponding to the point with coordinates (0,0) is 294 kN. In sequence, up to (0, 5000 days) the values of the critical load of buckling are 269, 248, 238, 227, 221, 217, and 214 kN, a variation corresponding to 27.27%.

The strains related to the ULS and subject to an axial loading corresponding to the critical buckling load are shown in Fig. 6. Thus, it is possible to verify their linear (or monotonic) aspect and that all strains are below the 2‰ normative limit (Karimi *et al.* 2013), defined as the strain at which concrete begins to crack (Tamayo *et al.* 2015). The maximum strain value corresponding to the critical buckling load, which was investigated under the most unfavorable condition, was 0.094‰, representing just 4.72% of that limit. These results were obtained by considering the total deformation of the structure, including

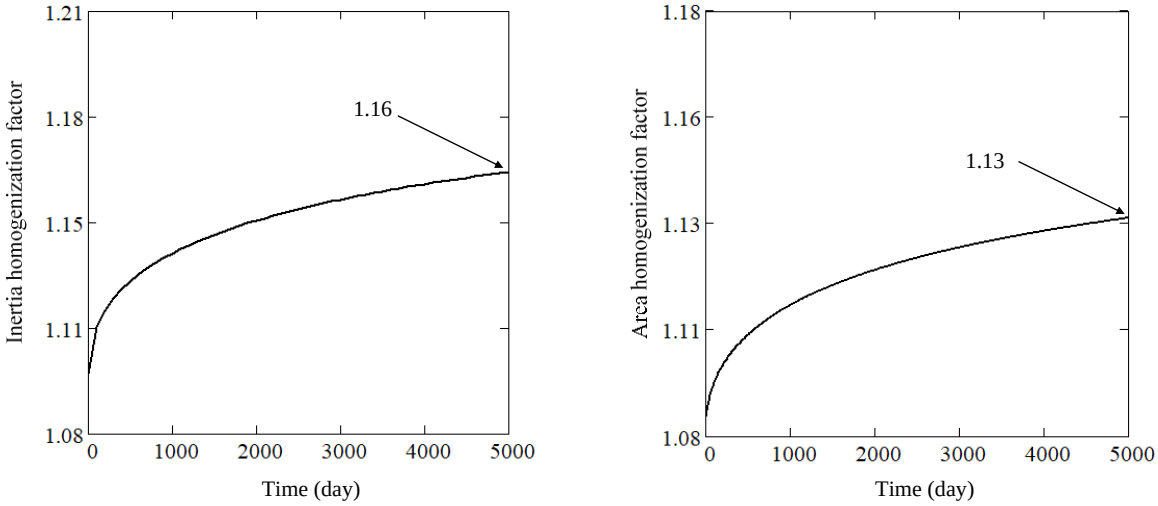

(a) Section S3.

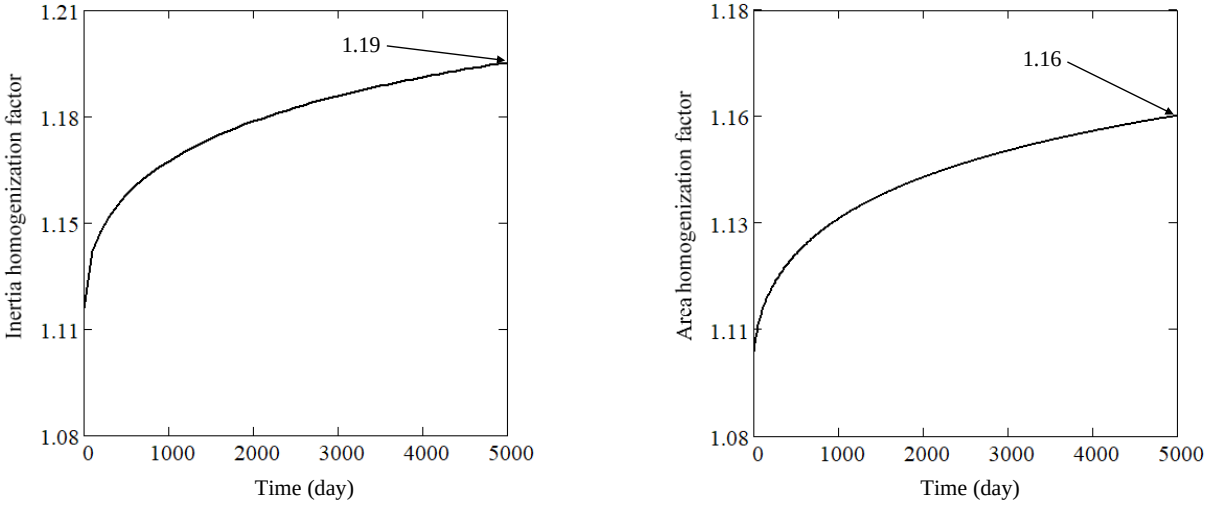

(b) Section S4

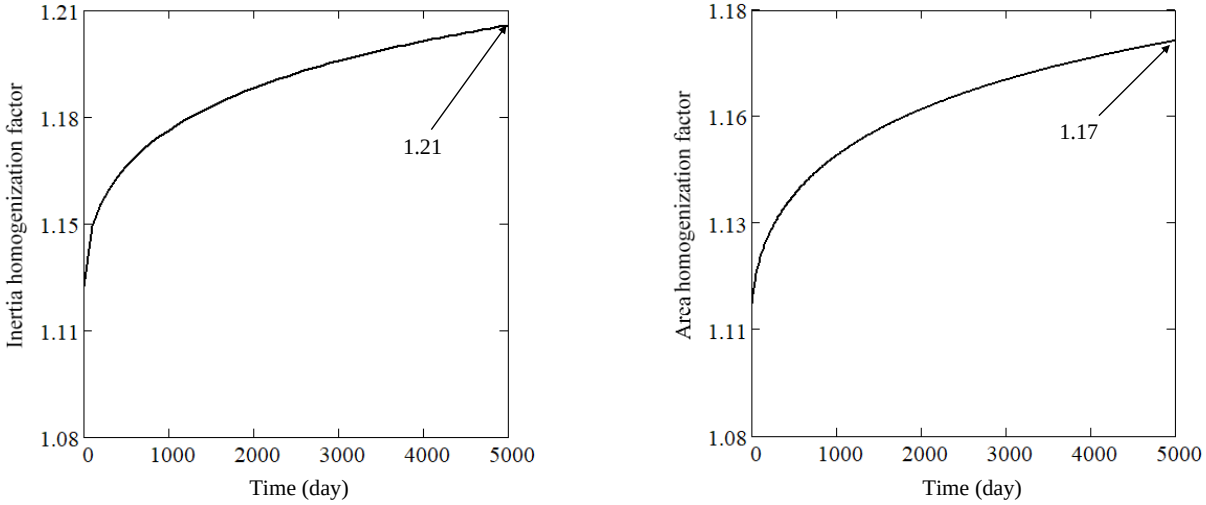

(c) Section S5

Fig. 7 Inertia (left) and area (right) homogenized factors over time

Table 1 Results with respect to time

Time	E	N_{cb}	ΔN_{cb}	FEM	ΔFEM	$\frac{\Delta N_{cb}}{FEM}$	f_{ctm}	ν_S^h ; ν_S^{st} (%)					
								$S3$ (ξ = 0.83%)		$S4$ (ξ = 0.99%)		$S5$ (ξ = 1.10%)	
(day)	(MPa)	(kN)	(%)	(kN)	(%)	(%)	(MPa)	ν_S^h	ν_S^{st}	ν_S^h	ν_S^{st}	ν_S^h	ν_S^{st}
0	19121	293.89	-	260	-	11.6	45.00	3.64	3.52	3.73	3.60	3.27	3.16
90	16964	269.11	- 8.43	232	-10.6	13.7	48.01	3.26	3.74	3.32	3.80	2.87	3.28
500	15131	248.05	- 7.82	208	-10.5	16.2	48.80	3.08	3.98	3.11	4.01	2.65	3.42
1000	14236	237.76	-4.15	196	-5.9	17.7	48.91	3.01	4.12	3.03	4.13	2.57	3.49
2000	13314	227.17	- 4.46	183	-6.5	19.5	48.97	2.94	4.27	2.95	4.27	2.48	3.58
3000	12784	221.08	- 2.68	175	-4.1	20.6	48.99	2.90	4.37	2.90	4.36	2.43	3.63
4000	12419	216.89	- 1.89	170	-2.9	21.5	49.00	2.87	4.45	2.87	4.42	2.40	3.67
5000	12145	213.74	- 1.45	166	-2.3	22.2	49.01	2.85	4.50	2.85	4.47	2.37	3.70
Δ % =	-36.48	-27.27	---	-36%	---	---	8.19	-15%	22%	-17%	19%	-21%	15%

E = modulus of elasticity (Eq. (1)); N_{cb} = critical buckling load (Eq. (35)); FEM = finite element method (Eq.(20)); f_{ctm} = resistance of concrete (Eq. (60)); Δ= difference at next instant of time; ν = normal reduced force (concrete, Eq. (58); reinforcement steel, Eq. (61)); ξ = reinforcement ratio; $S3$, $S4$, and $S5$ = cross-sections 3, 4, and 5, respectively

its foundation, which was calculated segment by segment using to Eq. (57), taking into consideration the homogenization of the concrete area. In Eq. (57), if creep in not considered in a specific cross-section, particularly $S1$ and $S2$, t should vanish from the corresponding portion in the summation, which lets n = 5 to be adopted.

$$\varepsilon^h(m_0,t)=\frac{\sum_{s=1}^{n}\Delta L_s}{L} \text{ with } \Delta L_s = \int_{L_{s-1}}^{L_s}\frac{\left[N_0(m_0)+\sum_{s+1}^{n}N_{s+1}+\bar{m}_s(x)(L_s-x)g\right]}{E_s(t)A_S^h(t)}dx \tag{57}$$

The evolution of the homogenizing factors for both inertia, Eq. (45), and area, Eq. (51), are depicted in Fig. 7.

To calculate stress on cross-section areas, the homogenizing factor took into consideration the relationship between the modulus of elasticity and the existing areas and the evolution of the concrete's strength. The non-dimensional axial load on homogenized concrete sections under creep effect can be obtained by

$$\nu_S^h(m_0,t)=\frac{N_S(m_0)}{A_S^h(t)\,f_{ctm}(t)} \tag{58}$$

where

$$N_S(m_0)=N_0(m_o)+\sum_{s+1}^{n}N_{s+1}+N_S^j \tag{59}$$

is the normal force acting on the section S, with

$$N_S^j=N_s/2 \text{ , for } s=3 \text{ and } 5; \quad \text{or} \quad N_S^j=N_s/4.5 \text{, for } s=4, \tag{60}$$

where N_s is the force related to the segment s as specified in Eq. (29), with s varying from 3 to 5, and n equal to 5, $A_S^h(t)$ is the homogenized cross-sectional area over time, given by Eq. (50), and $f_{ctm}(t)$ is a function representing the gain of concrete resistance over time, which is expressed by Eq. (60). The reduced normal force represented in Eq. (58) is a bilinear function, as shown in Fig. 8, where the inflection point at different times indicates the position of critical buckling load, at which the structure is at imminent collapse and no further load can be applied. The critical buckling load depends on time and is obtained using Eq. (35). When the normal force at the top is equal to the critical buckling force ($N_0(m_0)$=$N_{cb}(t)$), the relative stress values, given by Eq. (58), in homogenized concrete sections 3–5 are 3.64, 3.73, and 3.27%, respectively, at t = 0.

Therefore, the maximum value found for the stress in the homogenizing concrete area is close to 4% of the resistant capacity of the section (section $S4$).

When increasing the homogenized area of concrete, Eq. (51), the normalized stress decreases, as can be seen in Fig. 8, where zero time is the black curve, 90 days is the blue one, and so on up to 5000 days. That means the creep drives down the stress on the sections in favor of the ULS of the capacity resistance for vertical force, Fig. 8(left), and the limit of strain, Fig. 8(right). In relation to these aspects, the self-weight of the structure imposes initial values to the system. Fig. 9 shows the characteristic strength capacity of the concrete obtained using Eq. (60), which considers the evolution of concrete strength over time (t), as follows

$$f_{ctm}(t)=\left[\frac{t+t_0}{a+b\left(t+t_0\right)}\right]f_{cm28}\text{, in MPa,} \tag{61}$$

where a = 2.3 days, b = 0.917857, t_0 is time zero at the beginning of loading, therefore t_0 = 0 if this moment occurs 28 days after the casting of the concrete, and f_{cm28} is the compression resistance of concrete 28 days after its

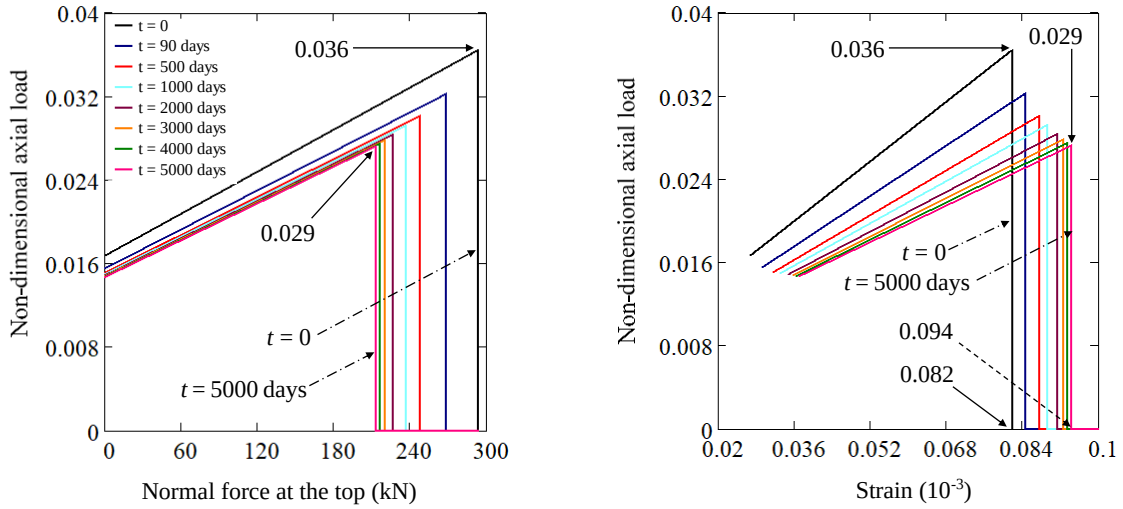

(a) Section S3.

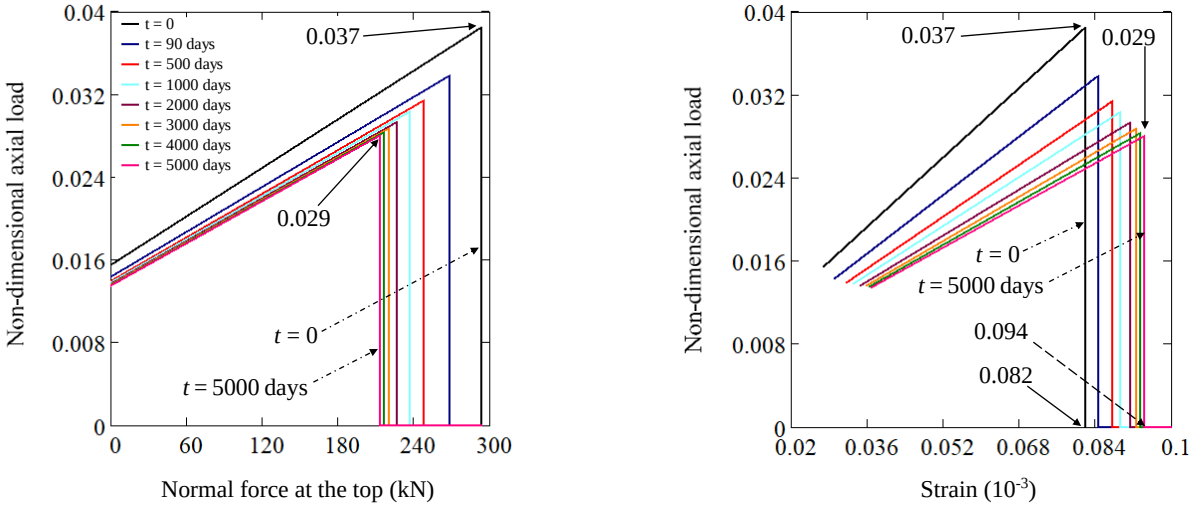

(b) Section S4

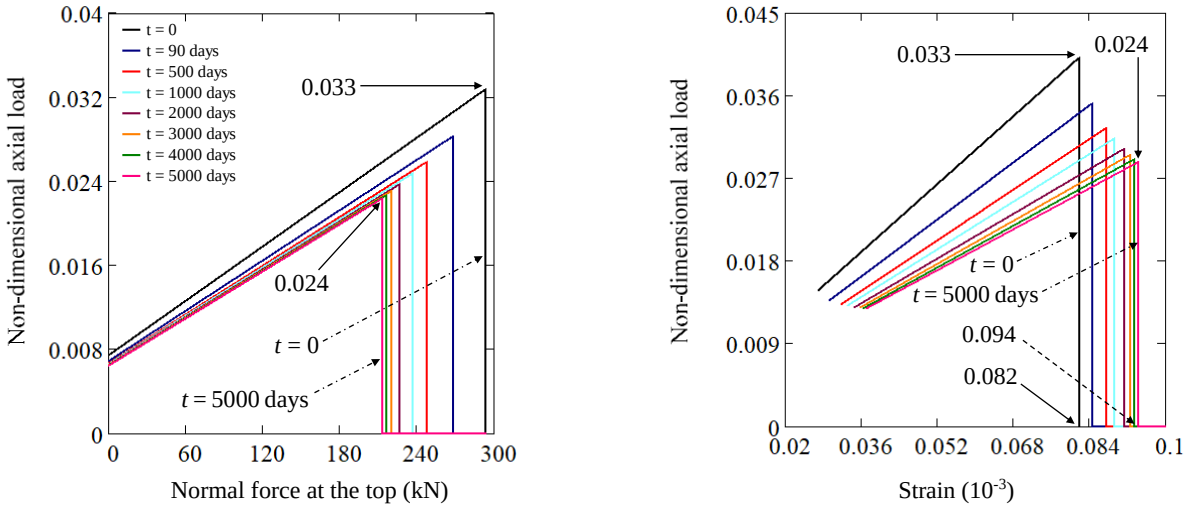

(c) Section S5

Fig. 8 Stress (left) and strain (right) on homogenized areas

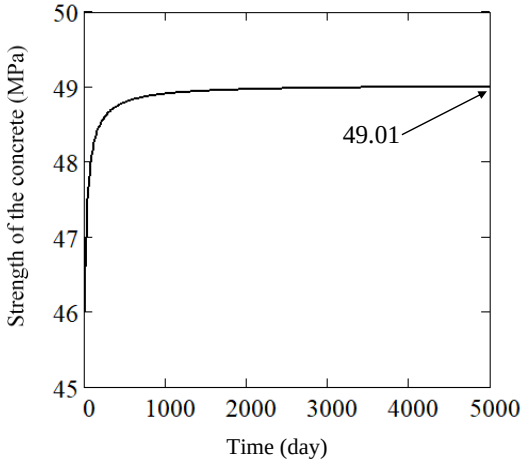

Fig. 9 Characteristic strength capacity of the concrete

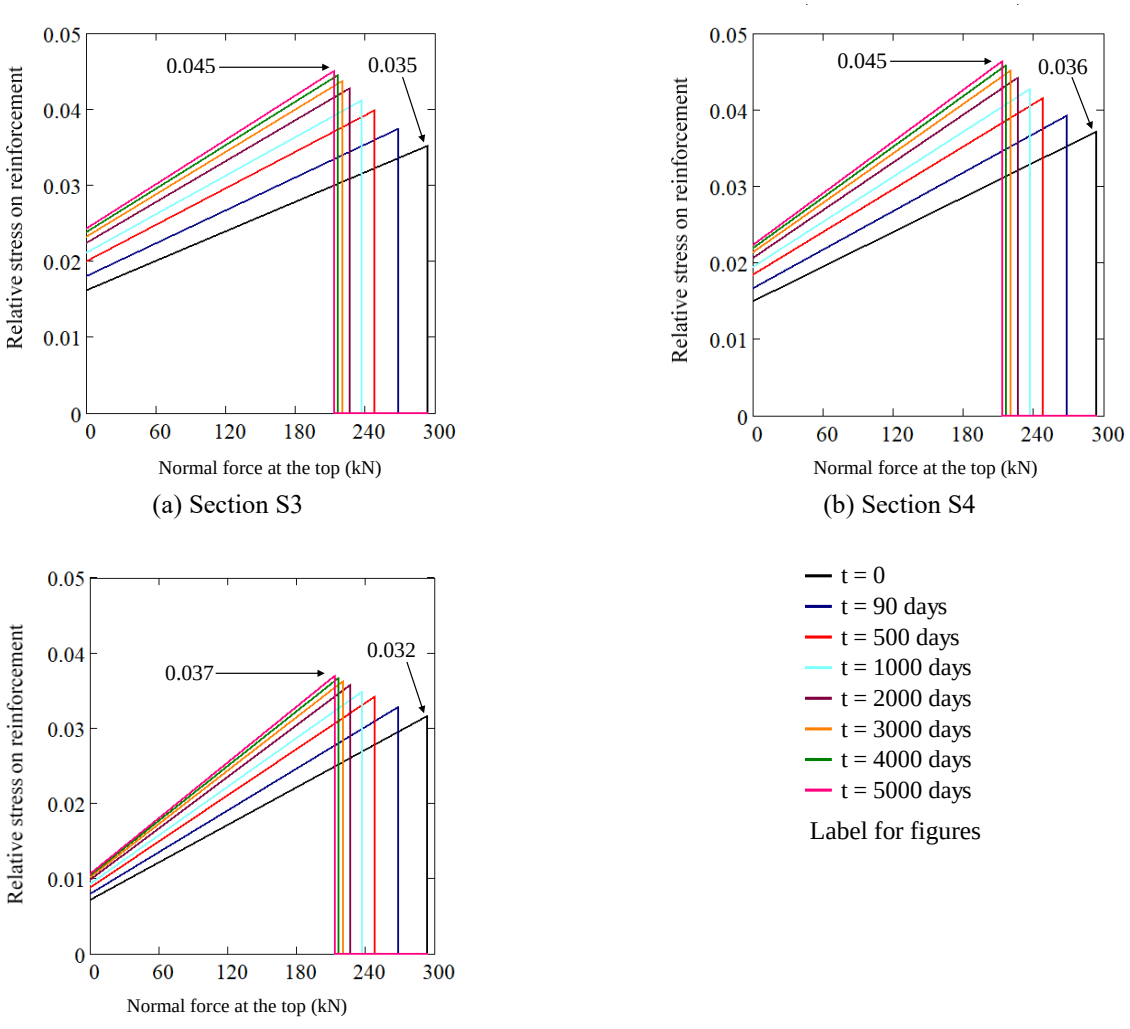

(a) Section S3

(b) Section S4

(c) Section S5

Fig. 10 Stress on reinforcement bar with normal force for each instant of time

production. The strength of the concrete stops growing at 5000 days in relation to the initial time.

In analogy to concrete, the relative force on the reinforcement steel is found as follows

$$\nu_S^{st}(m_0,t)=\frac{N_S^{st}(m_0,t)}{A_S^{st}f_y} \tag{62}$$

where A_S^{st} is the area, f_y is the yielding of steel, and N_S^{st} is force upon the steel area, which is given by Eq. (62)

$$N_S^{st}(m_0,t)=\frac{N_S(m_0)}{1+\frac{1}{\eta(t)}\frac{1}{\xi_S}} \tag{63}$$

where $N_S(m_0)$ is the normal force on section S given by Eq. (59), $\eta(t)$ is defined by Eq. (41), ξ_S represents the reinforcement rate of the considered section, with S varying from 3 to 5 for the present analysis. Eq. (62) represents the condition of force balance and the compatibility of displacements in a cross-section S. Fig. 10 plots Eq. (61) for a variation of the mass applied on top of the structure from zero up to the mass corresponding to the critical buckling load for each defined time.

Additionally, an internal balance existed, which compensated for the increasing strains caused by the applied loading as the concrete's modulus of elasticity decreased over time. Consequently, stress was transferred to the reinforcement in the sections as demonstrated in Fig. 11, which expresses the relationship between ν_S^h and ν_S^{st} as presented in Table 1. However, this additional stress, which was calculated over each bar according to Eq. (61), was far from producing the yielding of steel, as shown in Fig. 10. From the calculation with consideration to the self-weight of the superior segments, the following conclusions were drawn: in Section $S3$, the stress at the critical load was 22.52 MPa (4.50% of f_y); in Section $S4$, the same stress was 22.35 MPa (4.47% of f_y); in Section $S5$, the same stress was 18.50 MPa (3.70% of f_y); the stress required for the yielding of steel was f_y = 500 MPa. These results were obtained through the equilibrium of forces and compatibility of displacements in the cross-sectional area, for which the reinforcement ratio was considered. In all simulations, the reinforcement's modulus of elasticity was equal to 205 GPa, standard conditions of concrete production were applied, and the acceleration of gravity was 9.807 m/s^2.

All the results are presented in Table 1. Table 1 shows that the variation over time can be considered as the modulus of elasticity of concrete (E), critical buckling load of the structure (N_{cb}), the difference between the successive values of the critical load (Δ), and the normal reduced force (or normalized) (ν_S^h) of the homogenized concrete area defined by Eq. (58), the relative force on reinforcement (ν_S^{st}) defined by Eq. (61), and the reinforcement ratio (ξ) for the sections of interest.

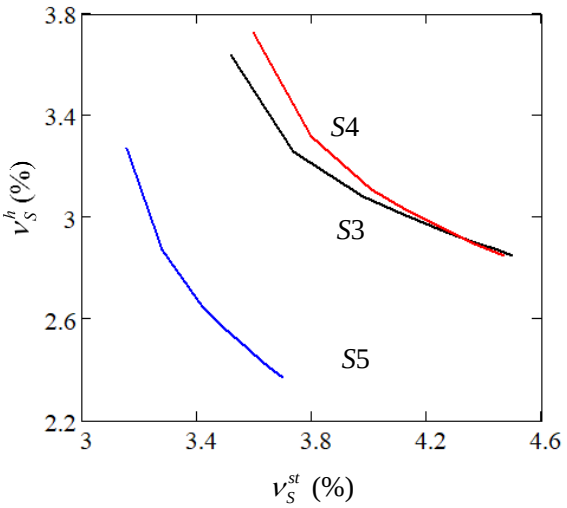

Fig. 11 Relationship between stresses on concrete and the reinforcement steel

An average difference of 18% for the elapsed time between the analytical procedure and FEM was found. This difference derives from the intrinsic properties of each mathematical method. The first one offers a solution that can be obtained directly in the continuum while the second one needs to discretize it. The analytical method tends to stiffen the structural system more than the solution by FEM, so the difference increases as the structure becomes more flexible by decreasing the modulus of elasticity. However, because the soil springs are not contemplated by the analytical shape function, FEM stiffens the lower segments of the structure more. Differences between analytical results and FEM were also noticed by Zhou *et al.* (2019) when studying the elastic buckling of columns with complex geometry. It can also be noted that multiplying the inertia reduction factor of 0.5 by the residual value of the modulus of elasticity of 0.64, the final averaged effective stiffness for the modulus of elasticity of concrete is 0.32. To find a final effective stiffness of 0.26 at the end of the period of convergence of the creep coefficient, a reduction factor of 0.4 should have to be applied to the modulus of elasticity of concrete at time zero.

7. Conclusions

The critical buckling force of an actual RC structure was analyzed using an analytical process based on vibration concepts for mechanical systems. The analyzed structure exhibited a geometrical variation throughout its height. The analysis considered all parameters required in the dynamic calculation. The geometric imperfections were considered with regard to the geometric stiffness. Cracks were considered with regard to the sections' factored moment of inertia. Finally, the viscoelastic behavior of concrete (or creep) was considered according to the ACI guidelines. The following conclusions were drawn based on the obtained results:

- The critical buckling load was determined as a compressive force of 294 kN at time zero, and 214 kN after 5000 days of applied loading, both of which correspond to the nullification of the first natural frequency, which marks a reduction of 27%.
- The modulus of elasticity exhibited a variation of 36.48% over the considered time due to creep.
- The strains exhibited linear behavior over time.
- All strains remained below the allowed axial deformation design limit (2‰), even when the buckling load was considered for each time. The maximum strain represents only 4.72% of this limit.
- The normal stresses exerted on the concrete homogenized cross-section decreased over time because the homogenizing factor increased.
- A maximum value of approximately 4% was determined using the relationship between the critical buckling load and the compressive capacity of the concrete homogenized section.
- Because part of the load was transferred to the reinforcement steel, the stresses reached a maximum of 4.50% of the steel yielding stress.
- The gain in the compressive strength of concrete over time was approximately 8.17% in the considered time span.
- This study only considered dead loads, such as the self-weight of the column, and a sustained lumped load at the top. Only characteristic values were considered, safety coefficients were not used.
- In the procedure described in this paper, an interactive or discretization process is not needed, and the solution of the critical buckling load can be accurately and directly obtained on the continuum.
- The mathematical process can be adapted to consider different geometries, with one or more, or even no lumped masses (and forces) along the height, which makes it possible to obtain approximate solutions to problems that can be modeled as unidimensional elements, such as buildings.
- In future work, comparative analyses with additional normative criteria for creep will be carried out for comparison, and the effects of transversal deformations and those induced by thermal variation will be considered along with creep. The effects of concrete shrinkage should also be studied. Moreover, further improvements will be made based on the reinforcement ratio of cross-sections and the structural slenderness ratio.

Acknowledgments

The author thanks RM Engineering Solutions for providing the data for the application case.

References

Abderezak, R., Daouadji, T.H., Abbes, B., Rabia, B., Belkacem, A. and Abbes, F. (2017), "Elastic analysis of interfacial stress concentrations in CFRP-RC hybrid beams: Effect of creep and shrinkage", *Adv. Concr. Constr.*, **6**(3), 257-278. https://doi.org/10.12989/amr.2017.6.3.257

Afefy, H.M. and El-Tony, El-T.M. (2016), "Simplified design procedure for reinforced concrete columns based on equivalent column concept", *Int. J. Concr. Struct. Mater.*, **10**(393). https://doi.org/10.1007/s40069-016-0132-0

American Concrete Institute ACI (2008), Prediction of creep, shrinkage, and temperature effects in concrete structures. ACI-209R-08, ACI Committee 209.

Awrejcewicz, J., Krysko, A.V., Zagniboroda N.A., Dobriyan, V.V. and Krysko, V.A. (2015), "On the general theory of chaotic dynamics of flexible curvilinear Euler–Bernoulli beams", *Nonlinear Dynam*., **79**(1), 11-29. https://doi.org/10.1007/s11071-014-1641-5.

Awrejcewicz, J., Krysko, V.A., Pavlov, S.P., Zhigalov, M.V., Kalutsky, L.A. and Krysko, A.V. (2019), "Thermoelastic vibrations of a Timoshenko microbeam based on the modified couple stress theory", *Nonlinear Dynam*., **99**(2). https://doi.org/10.1007/s11071-019-04976-w.

Banerjee, J.R. and Ananthapuvirajah, A. (2019), "An exact dynamic stiffness matrix for a beam incorporating Rayleigh-Love and Timoshenko theories", *Int. J. Mech. Sci*., **150**(2019), 337-347. https://doi.org/10.1016/j.ijmecsci.2018.10.012.

Bathe, K.J. and Wilson, E.L. (1973), "Solution methods for eigenvalue problems in structural mechanics", *Int. J. Numer. Methods Eng.*, https://doi.org/10.1002/nme.1620060207.

Bazant, Z.P. (1972), "Prediction of concrete creep effects using age-adjusted effective modulus method", *ACI Struct. J*., **69**(4), 212-219. DOI:10.14359/11265.

Bert, C.W. (1984), "Improved technique for estimating buckling loads", *J. Eng. Mech. - ASCE*, **110**(12), https://doi.org/10.1061/(ASCE)0733-9399(1984)110:12(1655)

Bert, CW. (1987), "Application of a version of the Rayleigh technique to problems of bars, beams, columns, membranes, and plates", *J Sound Vib*., **119**(2), DOI:10.1016/0022-460X(87)90457-3

B-Jahromi, A., Rotimi, A., Tovi, S., Goodchild, C. and Rizzuto, J. (2019), "Evaluation of the influence of creep and shrinkage determinants on column shortening in mid-rise buildings", *Adv. Concr. Constr.*, **5**(2), 155-171. https://doi.org/10.12989/acc.2017.5.2.155.

Bradford, M.A. and Gilbert, R.I. (1992), "Analysis of circular RC columns for short- and long-term deformations", *J. Struct. Eng. - ASCE*, **118**(3). https://doi.org/10.1061/(ASCE)0733-9445(1992)118:3(669).

Chaudhary, S., Pendharkar, U. and Nagpal, A.K. (2007), "An analytical-numerical procedure for cracking and time-dependent effects in continuous composite beams under service load", *Steel Compos. Struct*., **7**(3), 219-240. http://dx.doi.org/10.12989/scs.2007.7.3.219.

Clough, R.W. and Penzien, J. (1993), "Dynamics of Structures", McGraw-Hill International Editions, 2nd Edition, Taiwan.

Dezi, L., Gara, F. and Leoni, G. (2006), "Construction sequence modeling of continuous steel-concrete composite bridge decks", *Steel Compos Struct*., **6**(2), 123-138. http://dx.doi.org/10.12989/scs.2006.6.2.123.

Euler L. (1744), "De Curvis Elasticis, Additamentum I to his Methodus Inveniendi Lineas Curvas Maximi Minimive Proprietate Gaudentes", Lausanne and Geneva.

Fragiacomo, M., Amadio, C. and Macorini, L. (2002), "Influence of viscous phenomena on steel-concrete composite beams with normal or high-performance slab", *Steel Compos. Struct*., **2**(2), 85-98. http://dx.doi.org/10.12989/scs.2002.2.2.085.

Greenhill, A.G. (1881), "Determination of the greatest height consistent with stability that a vertical pole or mast can be made, and the greatest height to which a tree of given

proportions can grow", *Proceedings of the Cambridge Philosophical Society*, **4**, 65-73, London.

Jung, S.Y., Kim, N.I. and Shin, D.K. (2007), "Viscoelastic behavior on composite beam using nonlinear creep model", *Steel Compos. Struct.*, **7**(5), 355-376. http://dx.doi.org/10.12989/scs.2007.7.5.355.

Johnston, B.G. (1983), "Column buckling theory: Historic highlights", *J. Struct. Eng ASCE.*, **109**(9). https://doi.org/10.1061/(ASCE)0733-9445(1983)109:9(2086)

Karimi, K.; Tait, M.J.; El-Dakhakhni, W. W. (2013), "Analytical modeling and axial load design of a novel FRP-encased steel-concrete composite column for various slenderness ratios", *Eng. Struct.*, **46**(2013), 526–534. http://dx.doi.org/10.1016/j.engstruct.2012.08.016.

Kataoka L.T. and Bittencourt, T.N. (2014), "Numerical and experimental analysis of time-dependent load transfer in reinforced concrete columns", *Rev. IBRACON Estrut. Mater.*. **7**(5), http://dx.doi.org/10.1590/S1983-41952014000500003.

Kawano, A. and Warner, R.F. (1996), "Model formulations for numerical creep calculations for concrete", *J. Struct. Eng. ASCE*, **122**(3). https://doi.org/10.1061/(ASCE)0733-9445(1996)122:3(284).

Kumar, P. and Pratiher, B. (2019), "Modal analysis and dynamic responses of a rotating Cartesian manipulator with generic payload and asymmetric load", *Mech. Based Des. Struct.*, **48**(7), https://doi.org/10.1080/15397734.2019.1624174.

Leissa, A.W. (2005), "The historical bases of the Rayleigh and Ritz methods", *J. Sound Vib.*, **287**(4-5). https://doi.org/10.1016/j.jsv.2004.12.021.

Li, J., Huo, Q., Li, X., Kong, X. and Wu, W. (2014), "Dynamic stiffness analysis of steel-concrete composite beams", *Steel Compos Struct.*, **16**(6), 577-593. http://dx.doi.org/10.12989/scs.2014.16.6.577.

Lord Rayleigh (1877), *Theory of Sound*, New York: Dover Publications, re-issued.

Lubbers, L.A., van Hecke, M. and Coulais, C. (2017), "A nonlinear beam model to describe the post-buckling of wide neo-Hookean beams", *J. Mech. Phys. Sol.*, **106**(191-206). https://doi.org/10.1016/j.jmps.2017.06.001.

Madureira, E.L., Siqueira, T.M. and Rodrigues, E.C. (2013), "Creep strains on reinforced concrete columns", *Rev. IBRACON Estrut. Mater.*, **6**(4). http://dx.doi.org/10.1590/S1983-41952013000400003.

Marin, M.C. and El Debs, M.K. (2012), "Contribution to assessing the stiffness reduction of structural elements in the global stability analysis of precast concrete multi-story buildings". *Rev. IBRACON Estrut. Mater.*, **5**(3), 316–342. http://dx.doi.org/10.1590/S1983-41952012000300005

Maru, S., Asfaw, M. and Nagpal, A.K. (2001), "Consistent Procedure for Creep and Shrinkage Effects in RC Frames", *J Struct. Eng. - ASCE.*, **127**(7). https://doi.org/10.1061/(ASCE)0733-9445(2001)127:7(726).

Mehta, P.K., Monteiro, P.J.M. and Filho, A.C. (1994), "Concreto: estrutura, propriedades e materiais" (Concrete: Structure, properties and materials), *Ed. PINI*, São Paulo, Brasil, (In Portuguese).

Mirmiran, A., Shahawy, M. aqnd Beitleman, T. (2001), "Slenderness limit for hybrid FRP-concrete columns", *J. Compos. Constr.*, **5**(1). https://doi.org/10.1061/(ASCE)1090-0268(2001)5:1(26).

Murawski, K. (2017), "Technical stability of continuously loaded thin-walled slender columns", 1 Ed., Lulu Press, Inc., North Carolina.

Samral, R.M. (1995), "New analysis for creep behavior in concrete columns", *J. Struct. Eng. - ASCE.*, **121**(3). https://doi.org/10.1061/(ASCE)0733-9445(1995)121:3(399).

SAP2000 (2019), Analysis reference manual. Integrated software for structural analysis and design. Berkeley, California: Computers and Structures, Inc

Sharma, R.K., Maru, S. and Nagpal, A.K. (2004), "Simplified procedure for creep and shrinkage effects in reinforced concrete frames", *J. Struct. Eng. - ASCE.*, **130**(10). https://doi.org/10.1061/(ASCE)07339445(2004)130:10(1545).

Szyszkowski, W. and Glockner, P.G. (1985), "An incremental formulation of hereditary constitutive laws applied to uniaxial problems", *Int. J. Mech. Sci.*, **27**(9), 583-594. https://doi.org/10.1016/0020-7403(85)90074-8.

Tamayo, J.L.P., Morsch, I.B. and Awruch, A.M. (2015), "Short-time numerical analysis of steel-concrete composite beams", *J Braz. Soc. Mech. Sci. Eng.*, **37**(1097). https://doi.org/10.1007/s40430-014-0237-9.

Temple, G. and Bickley, W.G. (1933), "Rayleigh´s Principle and Its Applications to Engineering", Oxford University Press, Humphrey Milford, London.

Timoshenko, S.P. and Gere, J.M. (1961), *Theory of Elastic Stability*. 2nd Ed., New York: McGraw-Hill Book Company

Uzny, S. (2011), "An elastically supported geometrically nonlinear slender system subjected to a specific load in respect of bifurcational load and free vibrations", *Int. J. Bifurc. Chaos.*, **21**(10), 2983-2992. https://doi.org/10.1142/S0218127411030295.

Wahrhaftig, A.M., Brasil, R.M.L.R.F. and Balthazar, J.M. (2013), "The first frequency of cantilever bars with geometric effect: a mathematical and experimental evaluation". *J. Braz. Soc. Mech. Sci. Eng.*, https://doi.org/10.1007/s40430-013-0043-9.

Wahrhaftig, A.M. and Brasil, R.M.L.R.F. (2017), "Initial undamped resonant frequency of slender structures considering nonlinear geometric effects: The case of a 60.8 m-high mobile phone mast", *J. Braz. Soc. Mech. Sci. Eng.*, **39**(3), 725-735. https://doi.org/10.1007/s40430-016-0547-1.

Wahrhaftig, A.M. (2019), "Analysis of the first modal shape using two case studies", *Int. J. Comput. Meth.*, **16**(6). https://doi.org/10.1142/S0219876218400194.

Wahrhaftig, A.M., Silva, M.A. and Brasil, R.M.L.R.F. (2019), "Analytical determination of the vibration frequencies and buckling loads of slender reinforced concrete towers", *Lat. Am. J. Solids Stru.*, **16**(5). http://dx.doi.org/10.1590/1679-78255374.

Wang, T., Bradford, M.A. and Gilbert, R.I. (2006), "Creep buckling of shallow parabolic concrete arches", *J. Struct. Eng.*, **132**(10), 1641-1649. https://doi.org/10.1061/(ASCE)0733-9445(2006)132:10(1641).

Yaghoobi, H., Valipour, M.S., Fereidoon, A. and Khoshnevisrad, P. (2014), "Analytical study on post-buckling and nonlinear free vibration analysis of FG beams resting on nonlinear elastic foundation under thermo-mechanical loadings using VIM", *Steel Compos Struct.*, **17**(5), 753-776. http://dx.doi.org/10.12989/scs.2014.17.5.753.

Zhou, W., Li, Y., Shi, Z. and Lin, J. (2019), "An analytical solution for elastic buckling analysis of stiffened panel subjected to pure bending", *Int. J. Mech. Sci.*, **161**(162), https://doi.org/10.1016/j.ijmecsci.2019.105024.

Zienkiewicz, O.C, Watson, M. and King, I.P. (1968), "A Numerical method of visco-elastic stress analysis", *Int. J. Mech. Sci.*, **10**(1), 807-827. https://doi.org/10.1016/0020-7403(68)90022-2.

CC